Metals and Materials International (2018) 24:1149–1161
https://doi.org/10.1007/s12540-018-0069-8

Effects of Pre-ageing on Microstructure and Mechanical Properties of T9I6 Treated 2519A Aluminium Alloy

Lingying Ye[1,2] · Yu Dong[1,2] · Shengdan Liu[1,2] · Haichun Jiang[1,2,3] · Daxiang Sun[1,2] · Xinming Zhang[1,2]

Received: 13 December 2017 / Accepted: 8 March 2018 / Published online: 14 March 2018

Abstract
The effects of pre-ageing on the microstructure and mechanical properties of T9I6 treated 2519A aluminium alloy were investigated by hardness testing, tensile testing, transmission electron microscope, high resolution transmission electron microscope and differential scanning calorimetry. With the increase of pre-ageing time from 40 min to 4 h, the strength tends to increase first and then decrease; the pre-ageing time of 80 min results in the highest 0.2% proof strength and ultimate tensile strength of 491.9 and 513.8 MPa, respectively, and a high elongation of 14.6%. Pre-ageing is favorable for the formation of a number of primary GP zones, which can greatly improve the distribution of dislocations introduced by subsequent pre-deformation and secondary GP zones introduced by subsequent interrupted ageing. As a result, the number of precursors for θ′ hardening precipitates is maximized and the mechanical properties is improved after final re-ageing.

Keywords 2519A aluminium alloy · Pre-ageing · Mechanical properties · Microstructure

1 Introduction

2519A aluminium alloy with superior mechanical properties, weld ability and stress corrosion cracking resistance has been widely used as the primary material for many "moving structures", such as military aircrafts, helicopters and amphibious assault vehicle.

A number of investigations have been carried out on 2519A-T87 alloy and focused on its dynamic mechanical properties, constitutive equations, and evolution of the precipitates during high rate strain impact [1–3]. Due to increasing demands for higher protection and better flexibility in the military industry, it is desirable to further improve mechanical properties of 2519A alloy. Zhang et al. [4–6] found that the ultimate tensile strength of 2519A aluminium alloy can be increased to be 551 MPa by means of severe deformation with a reduction up to 80%. However, due to the severe plastic deformation, the ductility and toughness decrease significantly and may become unacceptable. Wang et al. [7, 8] found that the addition of rare earth elements can improve the distribution of fine θ' precipitates, and therefore increase the mechanical properties of 2519A aluminium alloy. Gu et al. [8, 9] found that interrupted ageing can improve the mechanical properties of 2519A aluminium alloy effectively. Interrupted ageing was initially proposed by Lumley and his co-workers in order to achieve a combination of high tensile properties and other acceptable properties in Al alloys [10–12], and some tempers including interrupted ageing such as T6I4 and T6I6 ('I' means interrupted ageing) have been developed. It was found that the ageing treatment called 'T9I6' process, which includes solution heat treatment, pre-ageing, cold rolling, low temperature ageing and then re-ageing, can improve the mechanical properties of 2519A aluminium alloy [8]. In this work, the effects of pre-ageing on mechanical properties of T9I6 treated 2519A aluminium alloy were investigated, and the reason was discussed based on microstructure examination by transmission electron microscope (TEM), high resolution transmission electron microscope (HRTEM) and differential scanning calorimetry (DSC). It can help to have better understanding of the relationship between microstructure and mechanical properties of Al-Cu alloys.

✉ Shengdan Liu
lsd_csu@csu.edu.cn; csuliusd@163.com

[1] School of Materials Science and Engineering, Central South University, Changsha 410083, China

[2] Collaborative Innovation Center of Advanced Nonferrous Structural Materials and Manufacturing, Central South University, Changsha 410083, China

[3] Institut für Metallkunde und Metallphysik, RWTH Aachen Universität, Kopernikusstr. 14, 52056 Aachen, Germany

2 Experimental Procedures

The raw material used in this investigation was an industrial 2519A-T87 aluminium alloy plate, and T87 treatment was made up of solution treatment, quenching, cold-rolling at a reduction rate of 7%, and then artificial ageing. The chemical compositions of this alloy are given in Table 1.

Figure 1 shows the schematic of T9I6 treatment process. After solution heat treatment (SHT) at 808 K for 2 h in an air furnace and quenching into room temperature water (~298 K), the samples were transferred immediately (within 1 min) to an air-circulated furnace with the temperature of 438 K for pre-ageing; after holding for various time, i.e., 40 min, 80 min, 2 h, 3 h and 4 h, respectively, they were quenched in room temperature water and then pre-deformed immediately by cold-rolling with a reduction of 15%. Subsequently, the samples were subjected to interrupted ageing at 338 K for 5 days and then re-ageing at 438 K. In the following sections, the samples pre-aged for various time are referred as PA-40 min, PA-80 min, PA-2 h, PA-3 h and PA-4 h, respectively.

Vickers hardness and tensile tests were carried out to reveal the effect of pre-ageing time on the mechanical properties of 2519A aluminium alloy. After polishing, the hardness of the aged samples was measured on a MV-10B testing machine with a load of a 3 kg and a dwell time of 15 s; the given hardness values were averaged over 7 indentations. The hardness of the samples of each state was tested immediately after treatment in order to minimize possible effect due to natural aging. Tensile specimens with a gauge length of 30 mm and a cross section of 2 mm × 10 mm were prepared and tested on MTS Landmark Servo-hydraulic Test System in the air at room temperature. The tensile direction was parallel to the rolling direction of the specimens, and a crosshead speed of 2 mm/min was used. For each condition three specimens were tested to give an average value.

DSC was used to estimate the volume fraction of GP zones in the aged samples. DSC measurement was performed using an ETZSCH-STA449C machine under argon atmosphere with a heating rate of 10 K/min between 313 and 693 K. The dimensions of the DSC specimens were 5 mm × 2.5 mm × 0.5 mm, and the mass was approximately 15 mg. The base line was measured and recalibrated after every three tests to minimize the possible influence and disturb from the environment.

Some discs with a diameter of 3 mm and a thickness of about 100 μm were prepared for microstructure examination by TEM and HRTEM. After electro-polishing in a HNO_3–CH_3OH solution (volume ratio of 3:7) at about 250 K using a voltage of 15 V, they were examined using a Tecnai G^2 F20 transmission electron microscope operated at 200 kV and an aberration-corrected FEI Titan G^2 60–300 microscope operated at 300 kV. The rolling direction-normal direction (RD-ND) section of the specimens was examined. All TEM images were taken with the electron beam parallel or close to the $[001]_{Al}$ zone axis which is the best orientation to observe and analyze θ′ precipitates in Al-Cu alloys, and quantitative analysis of precipitates was carried out in order to have better understanding of the microstructure.

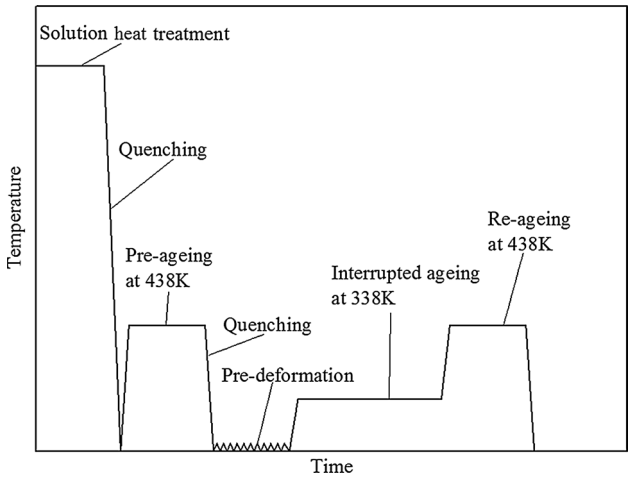

Fig. 1 Schematic of T9I6 treatment

3 Results

3.1 Hardness and Tensile Properties

Table 2 gives the Vickers hardness of samples PA-40 min, PA-80 min, PA-2 h, PA-3 h and PA-4 h of different state during T9I6 treatment. For the samples of pre-aged state, the hardness increases with the increase of time, which results from the formation of GP zones [5]. Pre-deformation results in an apparent increase in the hardness of the pre-aged samples. After subsequent interrupted ageing the hardness exhibits a further increase; however, the increment becomes minor when pre-ageing time is longer than 2 h.

The hardness can increase further after final re-ageing at 438 K, see Fig. 2, which shows the hardness evolution of the samples during re-ageing. For all the samples, the hardness tends to increase with the increase of time; however, the time to achieve the peak hardness and the hardness increment are affected by pre-ageing time, and this is because the

Table 1 Chemical compositions of the 2519A aluminium alloy (wt%)

Element	Si	Fe	Cu	Mn	Mg	Ni	Zn	Ti	Zr
Content	0.04	0.11	5.42	0.29	0.17	0.05	0.1	0.04	0.14

Table 2 Vickers hardness of samples PA-40 min, PA-80 min, PA-2 h, PA-3 h and PA-4 h at different states/HV3

Samples	Pre-aged state H_{pa}	Pre-deformed state, H_{pd}	Interrupted aged state, H_{ia}	Peak re-aged state, H_{pra}	Hardness increment $H_i = H_{pra} - H_{pd}$
PA-40 min	108.4 ± 2.2	121.0 ± 1.8	127.3 ± 3.0	142.5 ± 2.0	21.5
PA-80 min	117.4 ± 2.5	126.5 ± 2.1	137.1 ± 2.3	160.7 ± 3.2	34.2
PA-2 h	120.4 ± 2.1	137.5 ± 2.5	142.9 ± 3.0	155.3 ± 1.0	17.8
PA-3 h	127.2 ± 2.1	139.8 ± 1.5	141.3 ± 2.0	150.5 ± 3.0	10.7
PA-4 h	133.2 ± 2.6	146.2 ± 2.0	147.5 ± 4.0	152.1 ± 3.0	5.9

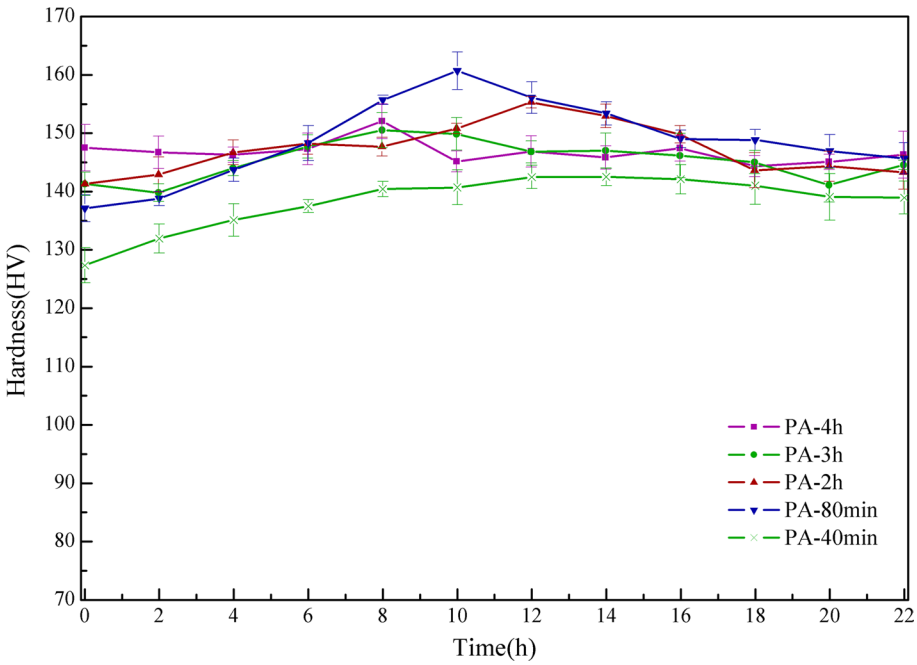

Fig. 2 Hardness evolution of samples PA-40 min, PA-80 min, PA-2 h, PA-3 h and PA-4 h during re-ageing at 438 K

microstructure is changed due to different pre-ageing time as discussed hereafter. With the increase of pre-ageing time from 40 min to 80 min, the peak hardness of the samples after re-ageing increases from 142.5 HV to 160.7 HV; and the peak hardness tends to drop with a further extension of the pre-ageing time (Table 2). The pre-ageing time of 80 min leads to the highest hardness increment after final re-ageing treatment.

The tensile properties of samples PA-40 min, PA-80 min, PA-2 h, PA-3 h and PA-4 h after final re-ageing treatment are given in Table 3, and the tensile properties of raw material 2519A-T87 samples are also shown for comparison. Compared with T87 treatment, T9I6 treatment gives rise to higher tensile properties of 2519A aluminium alloy. Sample PA-80 min has the highest tensile strength more than 500 MPa with a high elongation of 14.6%. After 80 min, with the increase of pre-ageing time, both the strength and elongation tend to decrease gradually but still higher than that of T87 sample. Therefore, 80 min is the optimal pre-ageing time to achieve the highest mechanical properties of 2519A aluminium alloy as shown in Fig. 2, Tables 2 and 3.

Table 3 Tensile properties of different samples after final re-ageing treatment

Sample	0.2% proof strength/MPa	Ultimate strength/MPa	Elongation/%
PA-40 min	434.1 ± 5.7	465.1 ± 6.5	15.4 ± 0.4
PA-80 min	491.9 ± 7.9	513.8 ± 8.5	14.6 ± 0.7
PA-2 h	466.6 ± 6.8	498.3 ± 7.1	13.8 ± 0.5
PA-3 h	468.8 ± 5.5	485.6 ± 6.1	13.6 ± 0.7
PA-4 h	462.1 ± 8.1	477.9 ± 8.7	13.4 ± 0.4
T87	430.3 ± 7.7	460.6 ± 8.4	9.3 ± 0.6

3.2 Microstructure

3.2.1 Microstructure After Final Re-ageing

Typical TEM images of samples PA-40 min, PA-80 min, PA-2 h, PA-3 h and PA-4 h after final re-ageing are shown in Fig. 3, and typical $[001]_{Al}$ selected area diffraction

pattern (SADP) of sample PA-80 min is shown in Fig. 4 as an example. In all the samples, there is a uniform distribution of needle-like precipitates, which are primarily θ′ hardening phase according to their clear diffraction spots in the SADP in Fig. 4. It is known that θ′ precipitates make contribution to high strength of Al-Cu alloys, and they are Cu-rich precipitates lying on {011} planes of the aluminium matrix and exhibit a thin plate shape. Figure 5 shows HRTEM image and FFT of θ′ precipitates. The θ′ precipitate has a thickness of about 3.5 nm and a diameter of about 23 nm. Due to the thin-plate like shape, diffraction spots of θ′ precipitates are often elongated as shown in Figs. 4 and

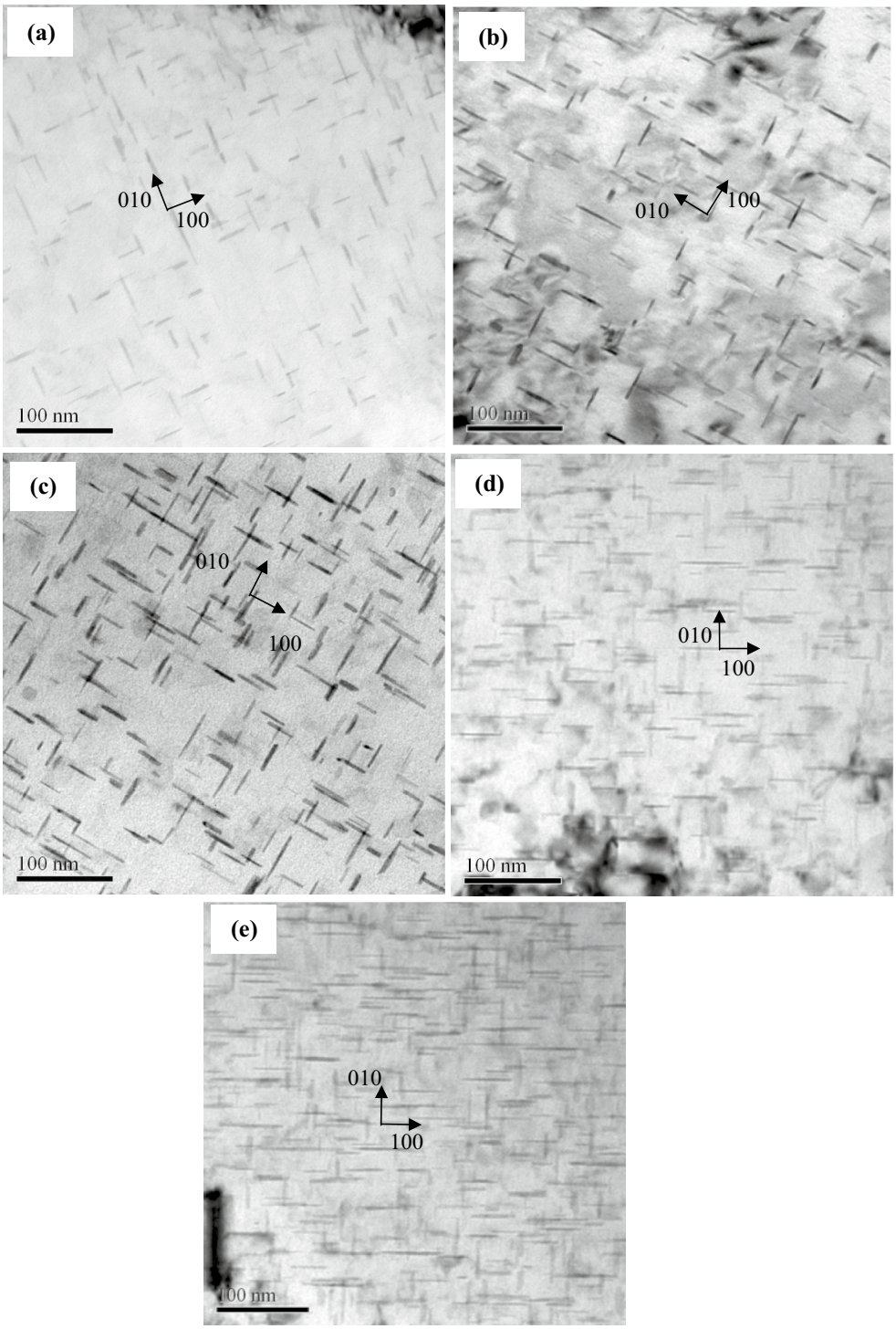

Fig. 3 Bright-field TEM images of samples **a** PA-40 min **b** PA-80 min **c** PA-2 h **d** PA-3 h and **e** PA-4 h after final re-ageing

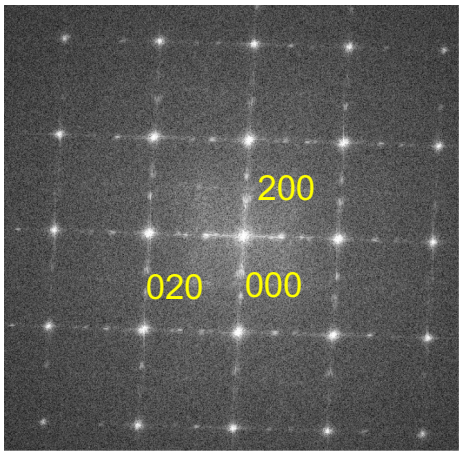

Fig. 4 Typical selected area diffraction pattern (SADP) of precipitates in the sample PA-80 min after final re-ageing

5. Few GP zones can be found in the matrix apart from θ′ precipitates.

The density of θ′ precipitates is lower in sample PA-40 min than other samples. With increasing the pre-ageing time from 40 min to 80 min, the density of θ′ precipitates tends to increase as shown in Fig. 3b. By comparing the Fig. 3c–e, it can be seen that further prolonging pre-ageing time has no significant influence on the density of θ′ precipitates but tends to increase their length. The length of a number of θ′ precipitates was measured and the distribution is shown in Fig. 6.

On the whole, the length of θ′ precipitates tends to increase with the increase of pre-ageing time; especially the proportion of θ′ precipitates with a length above 30 nm increases significantly after 80 min. In sample PA-40 min, the proportion of θ′ precipitates with a length of 30–40 nm is more than 15%; while in sample PA-80 min, the proportion of θ′ precipitates with a length above 30 nm is less than 5%, and also it has the largest proportion of θ′ precipitates with a length of 15–20 nm among the five samples. With the increase of pre-ageing time from 80 min to 4 h, the median average length of θ′ precipitates increase gradually.

3.2.2 Microstructure After Pre-ageing

A number of GP zones formed after pre-ageing, and they tended to grow and might transform into θ′ precipitates with the increase of pre-ageing time. Figure 7 shows TEM images of the samples after pre-ageing at 438 K for 40 min, 80 min and 4 h, respectively. After pre-aging for 40 min, there is a high density of GP zones with a length of about 5–15 nm and a thickness of about 0.8 nm in the matrix, see Fig. 7a, b. Prolonging the pre-aging time to 80 min results in slight coarsening of GP zones, see Fig. 7c, the length increases to about 10–20 nm with a thickness of about 1 nm; the diffraction streaks in the $<001>_{Al}$ direction due to GP zones become quite clear and sharp, see Fig. 7d. GP zones continue to coarsen and even transform into θ′ precipitates after further pre-aging; as shown in Fig. 7f, some blur spots due to θ′ precipitates may be seen in the sample after pre-ageing for 4 h at 438 K, indicating the presence of θ′ precipitates; the length of these precipitates is about 15–30 nm and the thickness is about 1.2 nm (Fig. 7e).

3.2.3 Microstructure After Interrupted Ageing

After interrupted ageing, fine GP zones formed in the samples. Figure 8 shows TEM images of samples PA-40 min,

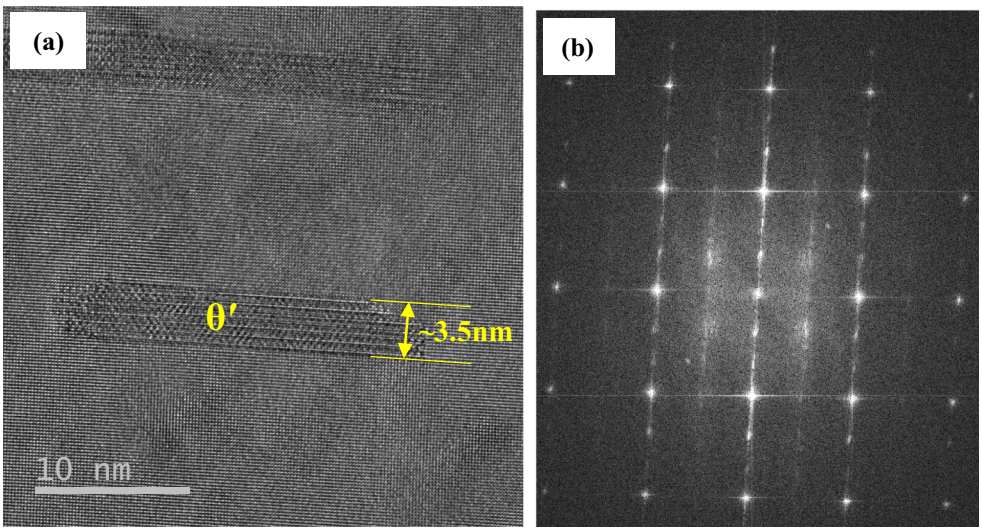

Fig. 5 **a** HRTEM image and **b** FFT of θ′ precipitates in the sample PA-80 min after final re-ageing

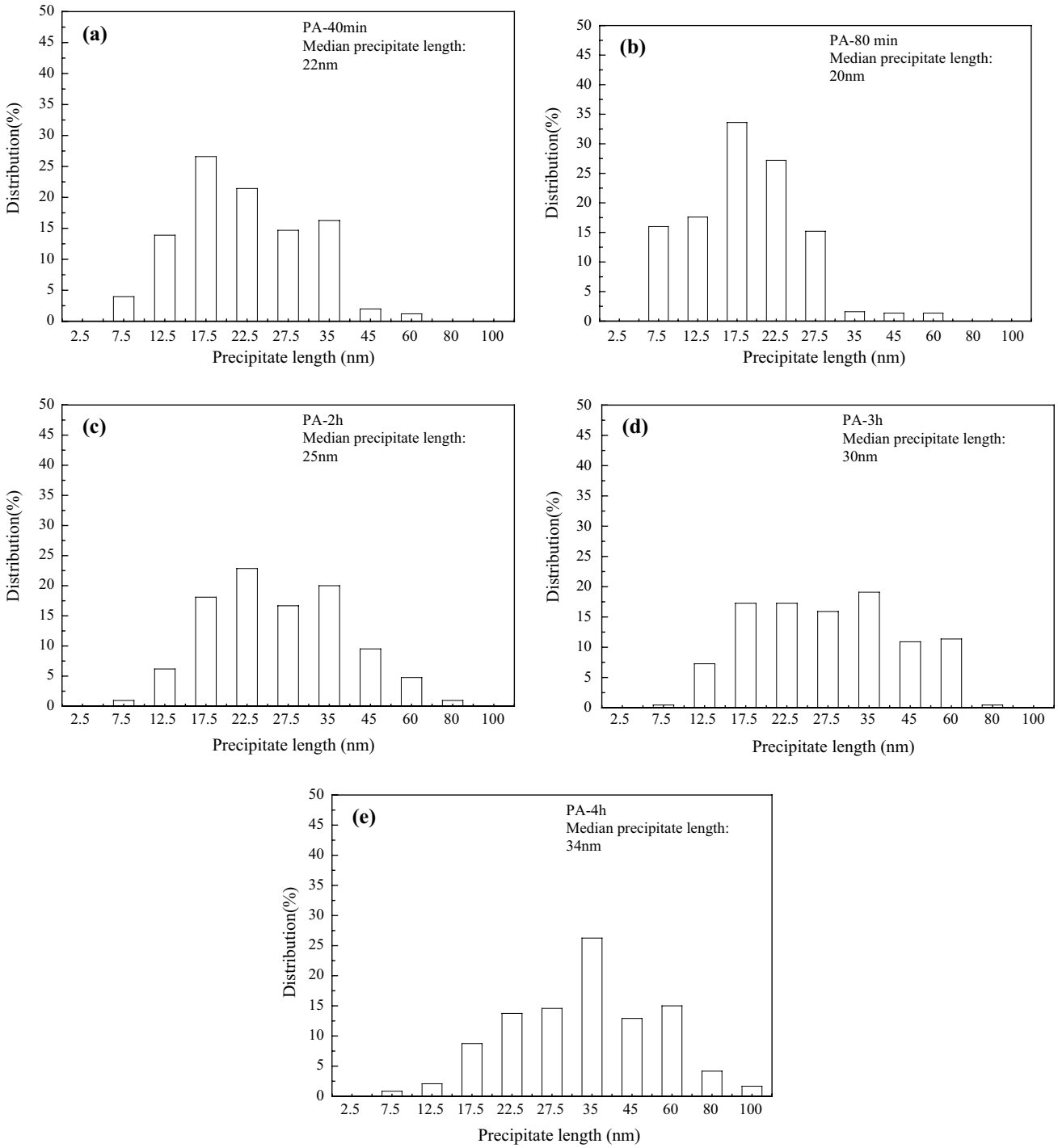

Fig. 6 Comparison of the distribution of lengths of θ′ precipitates in samples **a** PA-40 min, **b** PA-80 min, **c** PA-2 h, **d** PA-3 h and **e** PA-4 h after final re-ageing

PA-80 min and PA-2 h after interrupted ageing at 338 K for 5 days. The strain in the matrix around fine coherent GP zones are visible. In samples PA-40 min and PA-80 min after interrupted ageing, the average length of GP zones are about 4.0 nm and 4.2 nm, respectively, see Fig. 8a, b. Most GP zones are conventional single-atomic-layer zones from $[100]_{Al}$ [13], see HRTEM image in Fig. 9, some GP zones are indicated by arrows and they are coherent with the matrix. With the increase of pre-ageing time, GP zones tend to be larger and their density becomes lower. For

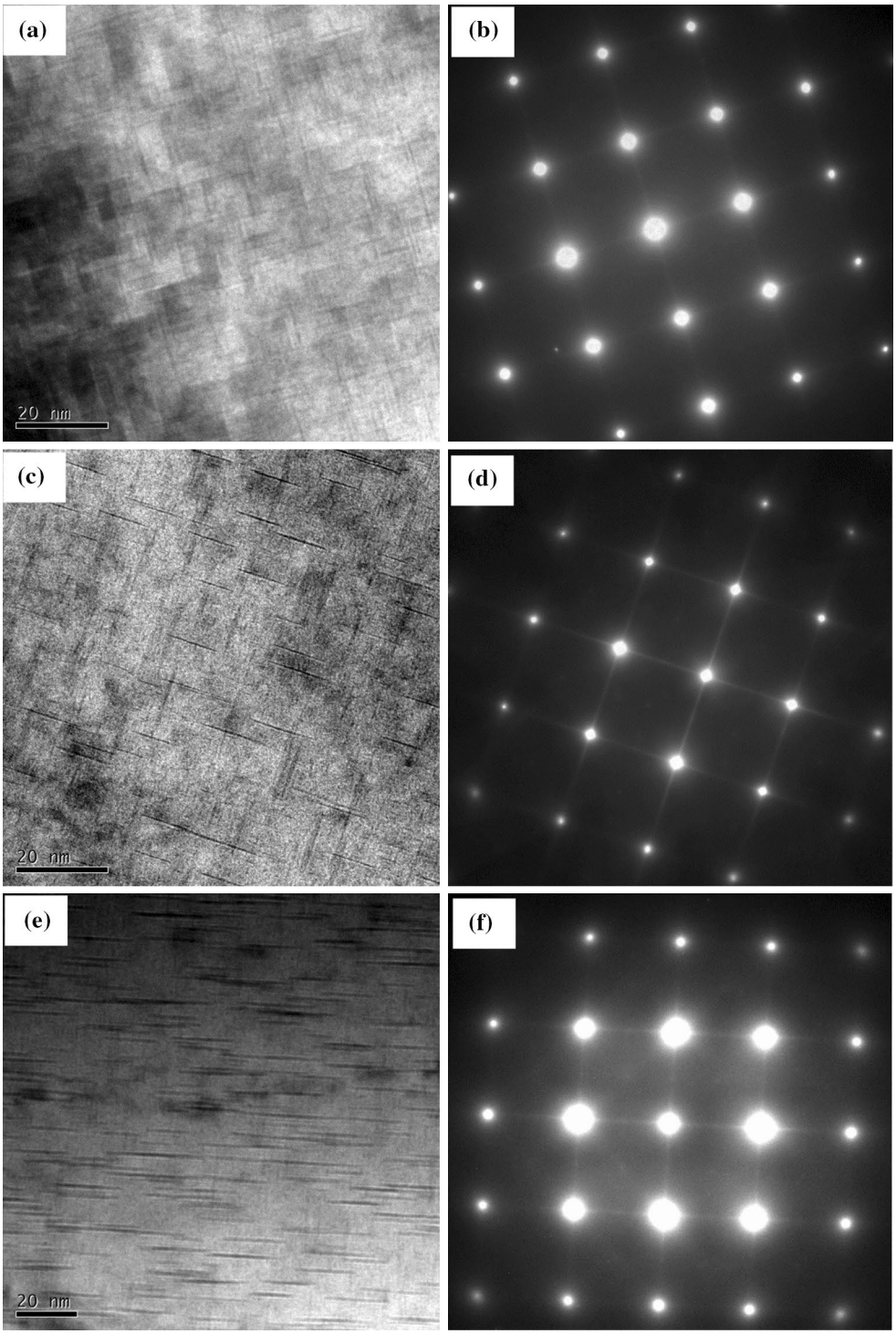

Fig. 7 Bright-field TEM images and SADP of precipitates in the samples after pre-ageing **a**, **b** PA-40 min **c**, d PA-80 min and **e**, **f** PA-4 h

instance, in the sample PA-2 h, it is observed that the average length of GP zones increases significantly to about 9.8 nm and the density decreases slightly, see Fig. 8c.

3.3 DSC Results

Typical DSC curves of different samples after interrupted ageing are shown in Fig. 10. For each curve, there is an obvious exothermic peak (marked by arrow A), which is

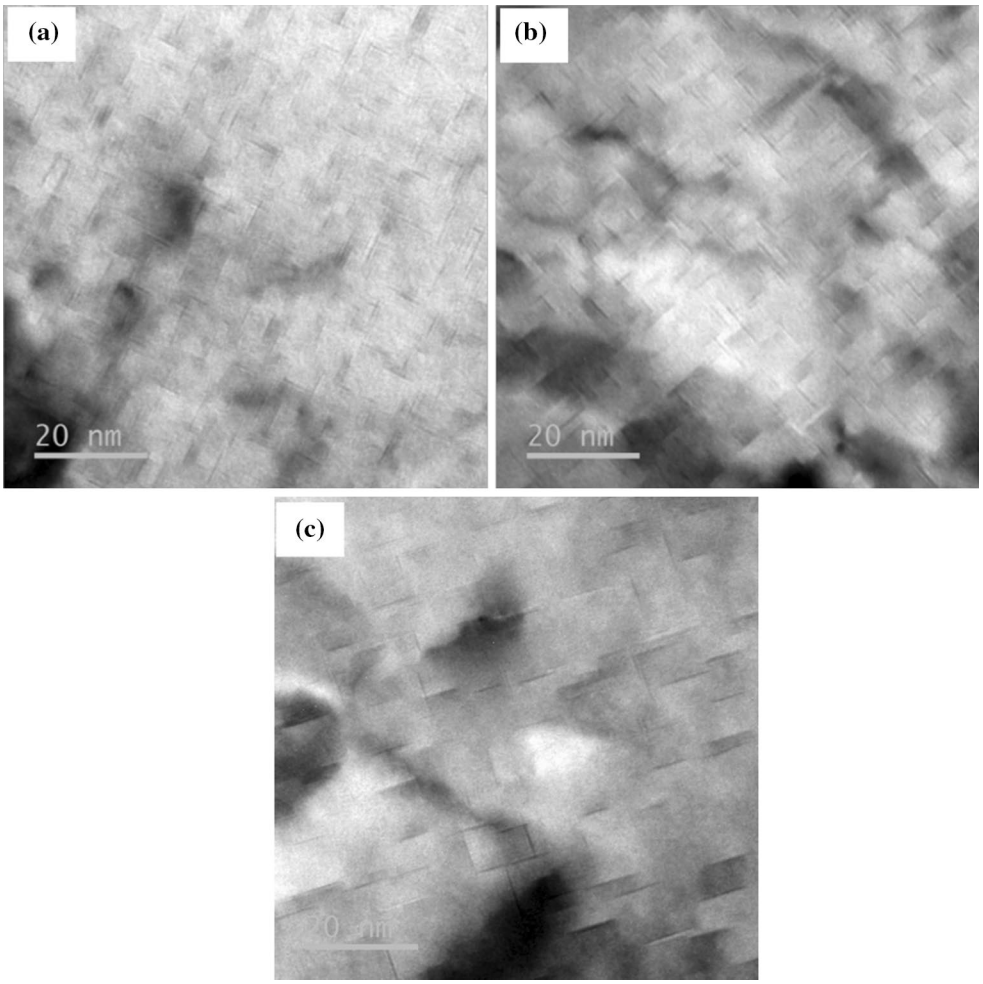

Fig. 8 TEM images of GP zones present in samples **a** PA-40 min, **b** PA-80 min and **c** PA-2 h after interrupted ageing

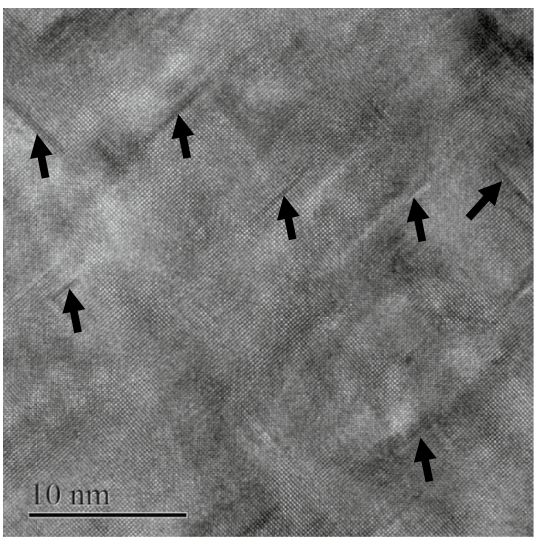

Fig. 9 HRTEM images of sample PA-80 min after interrupted ageing

likely due to the nucleation and growth of θ′ precipitates [14]. The peak temperatures of peak A of sample PA-40 min, PA-80 min, PA-2 h, PA-3 h and PA-4 h are about 518.2, 508.5, 514.0, 514.4 and 512.1 K, respectively. The peak temperature of peak A of sample PA-80mn is lower than that of other samples. Apart from peak A, a tiny endothermic peak (marked by arrow B) may be observed; it was magnified and shown in Fig. 11 so that it can be seen clearly. This peak is generally caused by the dissolution of GP zones [14]. Pre-ageing time alters the peak temperatures of peak B, which are about 475.9, 453.2, 473.7, 469.4 and 475.4 K, respectively, for the samples PA-40 min, PA-40 min, PA-2 h, PA-3 h and PA-4 h. These temperatures are higher than the pre-ageing and re-ageing temperature during T9I6 treatment.

In general, the enthalpy expressed by the area under the endothermic peak can indicate the volume fraction of second phase undergoing dissolution [15]. Therefore, the amount of GP zones in the samples after interrupted ageing can be compared according to the area of endothermic peak B in Fig. 11. However, reliable quantification of the area under

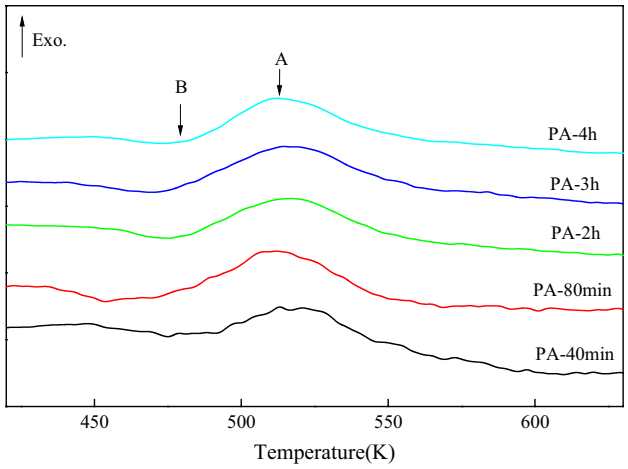

Fig. 10 Differential scanning calorimetry curves of the samples subjected to interrupted ageing at 338 K for 5 days

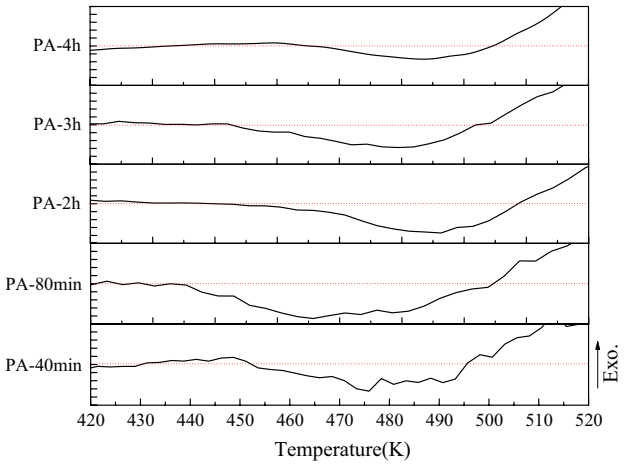

Fig. 11 Differential scanning calorimetry curves for comparison of peak B as a function of pre-ageing time for the samples after interrupted ageing at 338 K for 5 days

peak B requires a well-calibrated calorimeter and a stable baseline. During these tests, the baseline was checked and recalibrated after every three tests to ensure stability. The variation in the baseline was extremely small and had a negligible effect on the quantification. The area under peak B based on three tests is shown in Fig. 12. As the samples were subjected to pre-deformation, the heat liberated by recovery of the deformation structure or by possible GP zones formation during DSC testing may affect the area under peak B [16]. Another DSC scan was performed on samples after pre-deformation immediately after solution treatment (not shown here), and the maximum amount of solutes in supersaturated solid solution in these samples can ensure the largest driving force for GP zones formation. After DSC tests, no peak B could be observed. Therefore, these possible effects

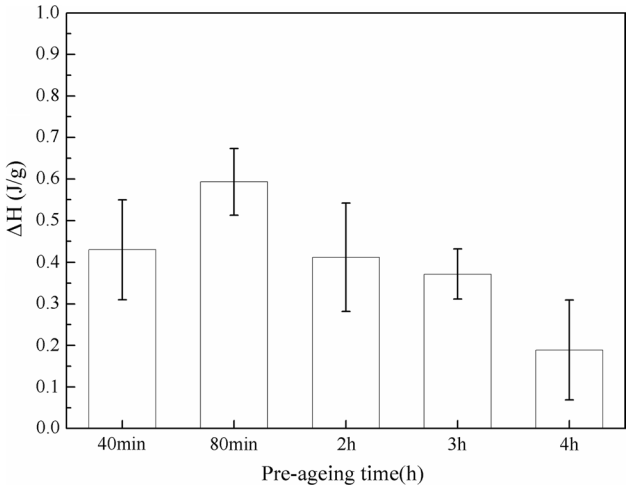

Fig. 12 The area under peak B in Fig. 10 as a function of pre-ageing time for the samples after interrupted ageing at 338 K for 5 days

can be negligible when compared with the heat absorbed by GP zones undergoing dissolution during DSC tests. From Fig. 12, it can be seen that the amount of GP zones tends to increase first with increasing pre-ageing time from 40 to 80 min, and then decrease gradually with the further increase of pre-ageing time to 4 h. Therefore, according to Figs. 8 and 12, it is believed that the volume fraction of GP zones is the highest in sample PA-80 min after interrupted ageing.

4 Discussion

A number of investigations have been carried out on ageing hardening of Al–Cu alloys, and the precipitation sequence of Al–Cu alloys during ageing below 438 K is generally as follows [17–19]:

$$Al_{ss} \rightarrow Al_{ss} + \text{GP zones} \rightarrow Al_{ss} + \theta' \rightarrow Al_{ss} + \theta$$

where Al_{ss} represents the aluminium supersaturated solid solution. It is known that metastable θ′ precipitates can lead to high strength [20–23]. As shown in Fig. 3, there is a uniform distribution of fine θ′ precipitates in all the samples, which therefore exhibit high hardness and high strength as shown in Tables 2 and 3. However, there is still significant difference in the hardness and strength between these samples subjected to pre-ageing for different time, and sample PA-80 min has the highest hardness and strength. For shear-resistant θ′ precipitates, the Orowan equation can be used for the estimation of strengthening increment, which is determined by precipitates size R and volume fraction V_f [19–23]. Precipitates with smaller R and higher V_f generally result in better strengthening effect, and therefore it is reasonable that the samples with finer and denser precipitates have higher strength. As shown in Fig. 3, θ′ precipitates have a plate-like

shape and exhibit a similar thickness but different length in the samples; from Fig. 6, it seems that a high proportion of θ′ precipitates with a length around 20 nm may lead to the highest strength. Moreover, it is critical to obtain a high density of θ′ precipitates.

In order to increase their density, it is essential to have an increased number of nucleation sites for θ′ precipitates. It is known that the nucleation of θ′ precipitates can occur on GP zones and dislocations [24, 25]. Therefore, it is reasonable to believe that a larger number of GP zones or dislocations are favorable for the formation of θ′ precipitates. For the T9I6 treatment shown in Fig. 1, all the parameters were the same except the pre-ageing time; and it is essential to understand how pre-ageing time affects the microstructure in the samples after interrupted ageing and after final re-ageing.

A large quantity of vacancies exists in the Al matrix after solution treatment and quenching, and GP zones can nucleate and grow during pre-ageing at 438 K. GP zones can retard movement of dislocations, and therefore the hardness tends to rise with the increase of pre-ageing time as shown in Table 2. The GP zones formed during pre-ageing are called primary GP zones hereafter. After subsequent pre-deformation, dislocations were introduced into the Al matrix, and they could interact with primary GP zones, leading to the formation of dislocation tangles [7, 8]. Moreover, the introduction of dislocations can result in dissolution of GP zones. For instance, Chen and his co-workers observed strain-induced dissolution of GP zones and about 50% GP zones dissolved in an Al-Cu alloy after deformation [26]. The reduction rate of cold rolling (15%) was not high, so dislocations might be localized in some regions; therefore, only part of GP zones dissolved after pre-deformation at room temperature. The dissolution of Cu-rich GP zones results in repartitioning of Cu atoms, which may interact with dislocation tangles and consequently strongly influence strain hardening. In Al-Cu solid solution, Cu atoms can stay at the dislocation–dislocation junction and enhance strain hardening [27, 28]. Moreover, the remnant primary GP zones can block the movement of dislocations, and a higher amount of primary GP zones after pre-ageing can retain more dislocations.

It was shown that pre-ageing is crucial for improving the distribution of dislocations and strengthening the dislocation–dislocation junction [4, 5, 8]. However, too long pre-ageing time may adversely influence the nucleation of GP zones during the interrupted ageing [29]. During interrupted ageing, the solute atoms diffuse slowly as the temperature (338 K) is low, and thus GP zones can nucleate and grow slowly and finally distribute uniformly in the matrix; the number of GP zones is higher compared to that in the samples after pre-ageing, as the hardness rises as shown in Table 2. The GP zones formed during interrupted ageing are called secondary GP zones hereafter. The Cu atoms at dislocation–dislocation junction can unlikely gather to form GP zones again at such a low temperature because it requires a high amount of activation energy to form coherent GP zones in lattice distortion area [4, 25]. And therefore, the nucleation rate of secondary GP zones mainly depends on the amount of supersaturated solute atoms in the Al matrix after pre-ageing. With the increase of pre-ageing time, supersaturated solute atoms are gradually consumed, primary GP zones coarse (Fig. 7) and depletion of solute atoms in the matrix occurs; this reduces the nucleation rate of secondary GP zones. Therefore, the time for pre-ageing must be selected carefully so that adequate solute atoms can be retained after quenching and pre-deformation for the formation of GP zones during subsequent interrupted ageing. In this work, the appropriate pre-ageing time is 80 min for the studied 2519A aluminium alloy, because the highest volume fraction of GP zones can be obtained, as shown in Figs. 8, 9, 10, 11 and 12.

The strength of 2519A aluminium alloy after T9I6 treatment is composed of matrix strength, precipitation hardening and strain hardening. The contribution of strain hardening to strength may be similar for all the samples because of the same reduction rate of cold rolling during pre-deformation. The primary GP zones formed after pre-ageing interact with dislocations introduced by pre-deformation, and increase the density of dislocations. Recovery may occur during interrupted ageing process [26, 28], but movement of dislocations is unlikely to occur due to the presence of primary GP zones. Precipitation hardening occurs during ageing, and a parameter H_i is introduced to discuss the age hardening and recovery effect, see Table 2. The H_i for sample PA-40 min is lower than that for sample PA-80 min, and H_i shows a decreasing trend with increasing pre-ageing time from 80 min to 4 h. When the pre-ageing time is short, the movement of dislocations cannot be blocked effectively because of few primary GP zones; as a result, recovery may occur during interrupted ageing. Therefore, recovery reduces strain hardening effect in sample PA-40 min and lowers H_i after age hardening treatment. For samples after pre-ageing for a time longer than 80 min, the effect of recovery can be negligible compared with the strength increment caused by strain hardening.

In order to better understand the effect of pre-ageing time, take samples PA-40 min, PA-80 min and PA-2 h as examples, the microstructure before and after interrupted ageing is schematically illustrated in Figs. 13, 14 and 15, respectively, and discussed in detail as follows.

For sample PA-40 min, the size of primary GP zones is smaller than that in sample PA-80 min, and this is shown in Fig. 7. Most Cu atoms were still in the Al matrix when the sample was pre-deformed by cold rolling. The dislocation–dislocation junctions cannot be strengthened by solute atoms, and the movement of dislocations may happen

during interrupted ageing. In the zone with a low density of dislocations, dislocations may be absorbed into dislocation tangles, and therefore some dislocations offset (Fig. 13); as a result, the dislocation density decreases. As strain hardening is mainly from dislocation tangles, the strengthening effect due to deformation decreases. Moreover, the movement

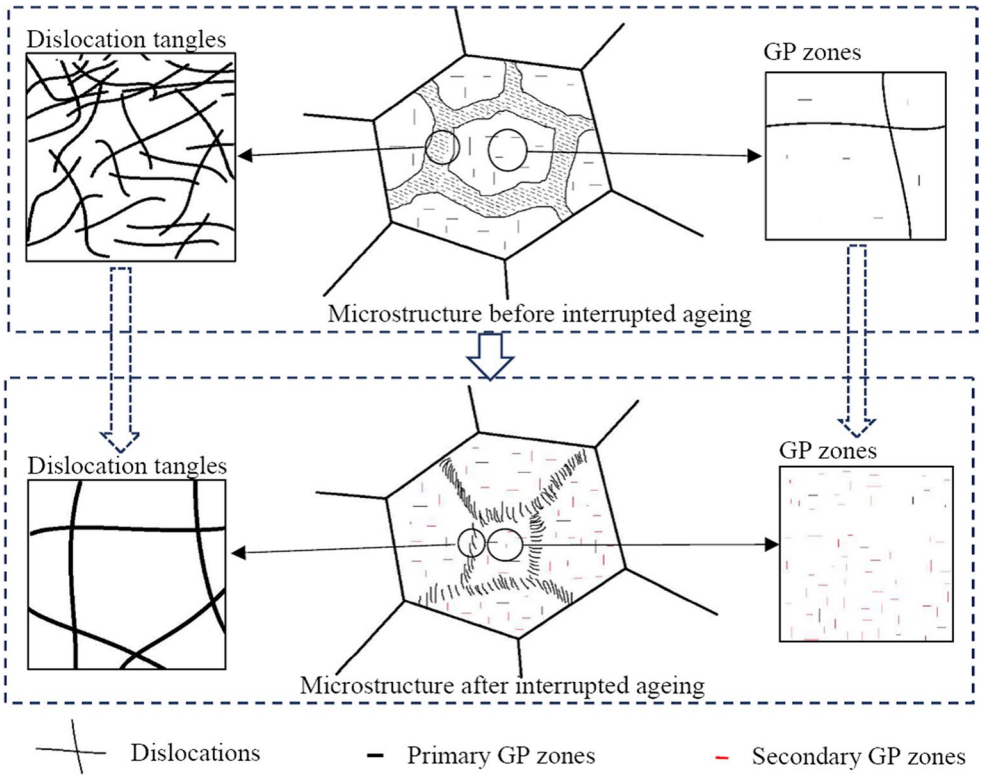

Fig. 13 Schematic of the microstructure in sample PA-40 min before and after interrupted ageing

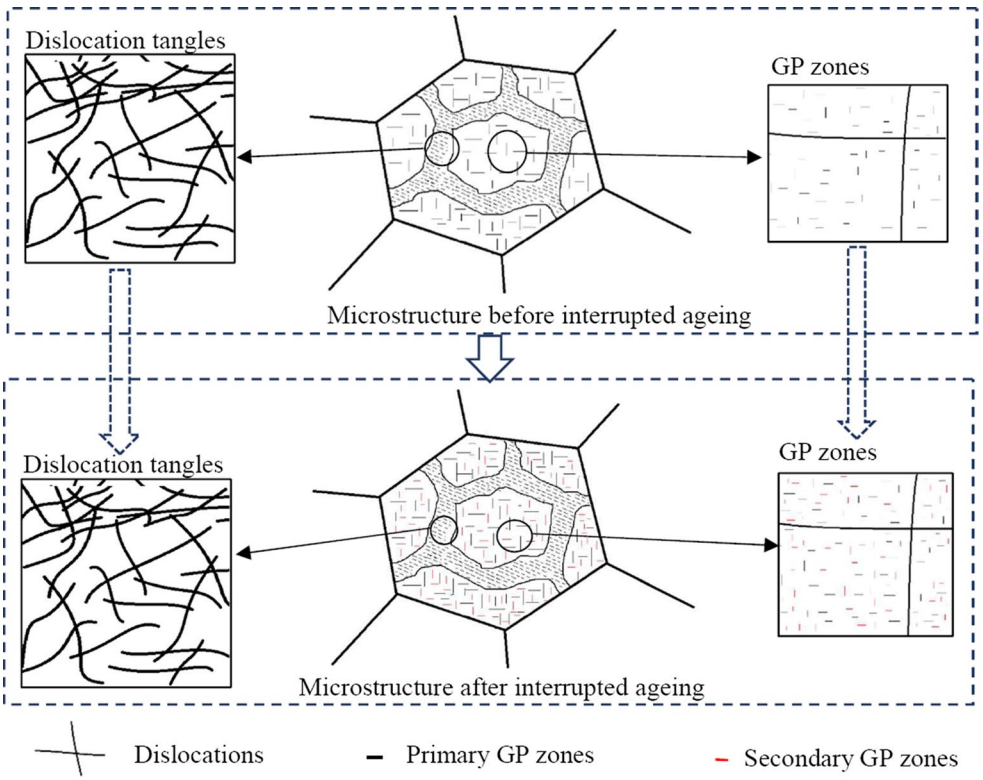

Fig. 14 Schematic of the microstructure in sample PA-80 min before and after interrupted ageing

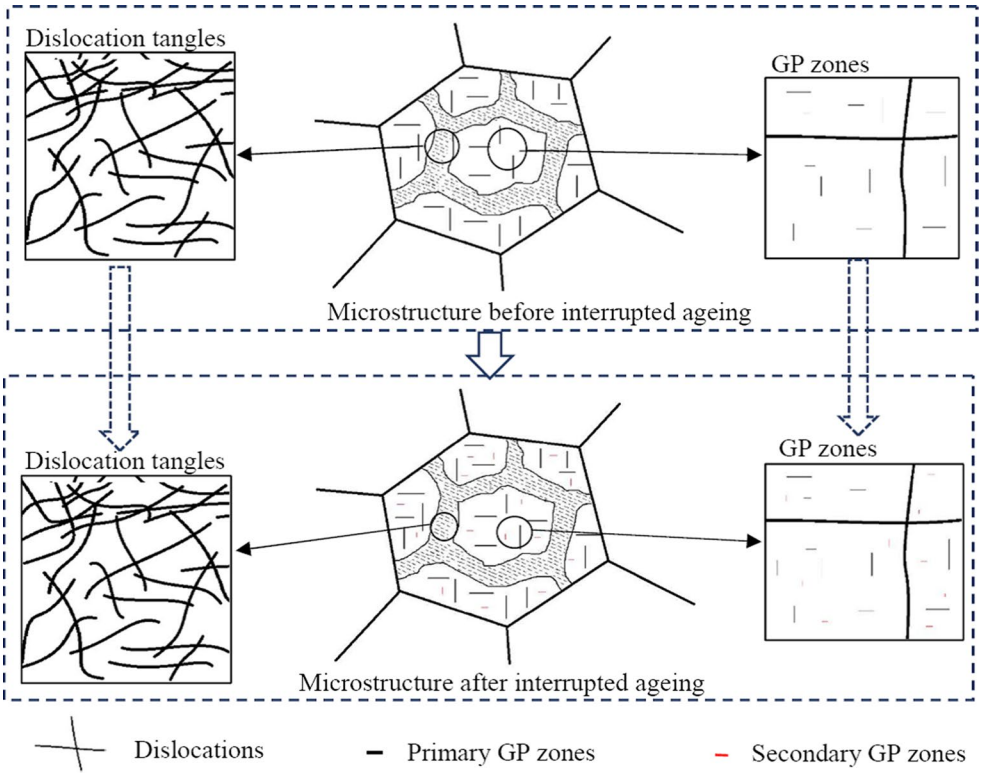

Fig. 15 Schematic of the microstructure in sample PA-2 h before and after interrupted ageing

of dislocation can reduce the amount of vacancies in the matrix, leading to fewer secondary GP zones during interrupted ageing. This can be seen from Table 2 that the hardness increment is smaller for the sample PA-40 min than PA-80 min after interrupted ageing.

Figure 14 is the schematic of the microstructure in sample PA-80 min before and after interrupted ageing. Before cold rolling, there is an adequate amount of primary GP zones with a proper size in the sample after pre-ageing for 80 min (Fig. 7). Strain-induced dissolution occurred and dislocation tangles formed after cold rolling. During interrupted ageing, there was a high amount of supersaturated solute atoms available for the formation of a large quantity of secondary GP zones, and the ΔH is the highest in this sample, see Fig. 12. As a result, there was a significant hardness increment after interrupted ageing (Table 2). During subsequent re-ageing, the fine and dense GP zones and dislocations can act as nucleation sites for θ′ precipitates. Consequently, the microstructure is optimized (Figs. 3, 4, 5 and 6) and the highest strength can be achieved (Table 2); the mechanical properties are also significantly higher than that of T87 temper.

From Table 2, the hardness tends to drop with the further increase of pre-ageing time. If the sample is pre-aged at 438 K for a longer time, the primary GP zones grow and even coarsen (shown in Fig. 7). Because of the interaction with dislocations during pre-deformation, a number of primary GP zones dissolve into dislocation–dislocation junction. After subsequent interrupted ageing, it can be seen from Fig. 8 that few fine secondary GP zones exist in the sample PA-2 h, and the coarse GP zones are likely primary GP zones. Figure 15 shows schematic of the microstructure in sample PA-2 h before and after interrupted ageing. If the pre-ageing time is further prolonged, fewer secondary GP zones can form. This can explain why there is only a slight increment in hardness for the samples PA-2 h, PA-3 h and PA-4 h after interrupted ageing (Table 2). The coarsening of primary GP zones leads to a larger size of θ′ precipitates, as shown in Figs. 3 and 6, and consequently strength tends to drop gradually with the further increase of pre-ageing time beyond 80 min.

5 Conclusion

1. For T9I6-treated 2519A aluminium alloy, the strength tends to increase first and then drop with the increase of pre-ageing time. The optimal pre-ageing time is 80 min, which results in the highest 0.2% proof strength and ultimate tensile strength of 491.9 and 513.8 MPa, respectively, and a high elongation of 14.6%. The mechanical properties are significantly higher than that of T87 temper.
2. The pre-ageing for 80 min gives rise to an optimized microstructure of primary GP zones with a proper amount and size, and consequently dislocation tangles

can be retained and a number of secondary GP zones can form after subsequent pre-deformation and interrupted ageing. As a result, the nucleation sites for θ′ hardening precipitates can be maximized during final re-ageing, and therefore the highest mechanical properties can be achieved.

Acknowledgments This study is supported by the National Key Research and Development Program of China (No. 2016YFB0300901), the Shenghua Yuying Project of Central South University (20130603) and China Scholarship Council Program (201706375013).

References

1. Z.G. Gao, X.M. Zhang, M.A. Chen, Scrip. Mater. **59**, 983 (2008)
2. Z.G. Gao, X.M. Zhang, M.A. Chen, J. Alloy. Compd. **476**, L1 (2009)
3. X.M. Zhang, H.J. Li, H.Z. Li, H. Gao, Z.G. Gao, Y. Liu, B. Liu, Trans. Nonferrous Met. Soc. China **18**, 1 (2008)
4. X. Zhang, L. Liu, Y.Z. Jia, Chin. J. Nonferrous Met. **20**, 1088 (2010)
5. H.Z. Li, X.P. Liang, M.A. Chen, X.M. Zhang, Trans. Mater. Heat Treat. **29**, 86 (2008)
6. Y.L. Zheng, B. Ji, L.Y. Ye, J. Cent, South Univ. Technol. (Nat. Sci.) **44**, 4806 (2013)
7. W.T. Wang, X.M. Zhang, Z.G. Gao, J. Alloy Compd. **491**, 366 (2010)
8. G. Gu, L.Y. Ye, H.C. Jiang, D.X. Sun, P. Zhang, X.M. Zhang, Trans. Nonferrous Met. Soc. China **24**, 2295 (2014)
9. L.Y. Ye, G. Gu, X.M. Zhang, Mater. Sci. Eng. A **590**, 97 (2014)
10. R.N. Lumley, I.J. Polmear, A.J. Mprton, Mater. Sci. Technol. **19**, 1483 (2003)
11. R.N. Lumley, I.J. Polmear, A.J. Mprton, Temper developments using interrupted ageing. in *Proceedings of the 9th International Conference on Aluminium Alloys*, (Institute of Materials Engineering Australasia Ltd, Brisbane 2004), pp. 85–95
12. R.N. Lumley, I.J. Polmear, A.J. Mprton, Mater. Sci. Technol. **21**, 1025 (2005)
13. M. Takeda, Y. Maeda, A. Yoshida, Scrip Mater. **41**, 643 (1999)
14. Y.P. Wu, L.Y. Ye, Y. Jia, Trans. Nonferrous Met. Soc. China **24**, 3076 (2014)
15. M.J. Starink, Int. Mater. Rev. **49**, 191 (2004)
16. N. Gao, M.J. Starink, N. Kamp, J. Mater. Sci. **42**, 4398 (2007)
17. G. Zlateva, Z. Martinova, *Microstructure of Metals and Alloys—An Atlas of Transmission Electron Microscopy Images* (CRC Press, NewYork, 2008), pp. 93–96
18. S.K. Son, M. Takeda, M. Mitome, Mater. Lett. **59**, 629 (2005)
19. V. Vaithyanathan, C. Wolverton, L.Q. Chen, Acta Mater. **52**, 2973 (2004)
20. S.R. Li, S.C. Zhou, *Heat Treatment of Metals* (Central South University Press, Changsha, 2005), pp. 198–202
21. J. Da costa teixeira, D.G. Cram, L. Bourgeois, T.J. Bastow, A.J. Hill, C.R. Hutchinson, Acta Mater. **56**, 6109 (2008)
22. L.M. Brown, R.K. Ham, *Strengthening Methods in Crystals* (Applied Science Publishers, London, 1971), pp. 32–39
23. A.J. Ardell, Metall. Trans. A **16**, 2131 (1985)
24. J.M. Fragomeni, B.M. Hillberry, Acta Mech. **138**, 185 (1999)
25. D.A. Porter, K.E. Easterling, M. Sherif, *Phase Transformations in Metals and Alloys*, 3rd edn. (CRC Press, Boca Raton, 2009), pp. 120–135
26. Y. Chen, M. Weyland, C.R. Hutchinson, Acta Mater. **61**, 5877 (2013)
27. Y. Estrin, *Dislocation Density-related Constitutive Modeling, Unified Constitutive Law of Plastic Deformation* (Academic Press, SanDiego, 1996), pp. 69–106
28. R. Øyvind, H.I. Laukli, B. Holmedal, Metall. Mater. Trans. A **37**, 2007 (2006)
29. J. Buda, R.N. Lumley, A.G. Croskey, K. Hono, Acta Mater. **55**, 3015 (2007)